MRS Advances (2025) 10:2396–2402
https://doi.org/10.1557/s43580-025-01407-4

ORIGINAL PAPER

Alloying-modulated strengthening behavior of Cu–xAg/Ni multilayer systems

Xi Li[1] · Thomas Kreuter[2] · Xuemei Luo[3] · Guangping Zhang[3] · Ruth Schwaiger[1]

Received: 15 August 2025 / Accepted: 7 October 2025 / Published online: 20 October 2025

Abstract

Cu–xAg/Ni multilayers (x = 0 at.%, 5 at.%, 10 at.%) with individual layer thickness of 25 nm were synthesized to explore alloy-modulated strengthening effects in nanolayered composites. Nanoindentation measurements revealed that alloying the Cu layers with 5 at.% and 10 at.% Ag increases the hardness of the Cu/Ni multilayer system by 10.4% and 12.9%, respectively. Microstructural characterization indicates that the solid solution of Ag atoms in the Cu matrix leads to lattice expansion and a corresponding increase in lattice mismatch at the Cu–xAg/Ni interfaces. Additionally, nanoscale Ag-rich precipitates were observed, resulting from the partial demixing of Ag in the Cu–Ag layers. The enhanced mechanical strength is attributed to a combination of strengthening mechanisms, including solid solution strengthening, precipitation hardening, and interface strengthening. Among these, theoretical analysis identifies lattice misfit strengthening at the interface as the predominant contributor to the overall hardening effect.

Introduction

Nanoscale multilayer composites have demonstrated remarkable mechanical [12, 18], magnetic [14] and electrical properties [1], as well as radiation resistance [11, 15]. These features have enabled their application in both structural and functional components, including magnetic sensors, biomedical sensing devices, nanoelectromechanical systems (NEMS), and functional coatings. In recent research, for example, the metal and E-glass/epoxy multilayers utilized in printed circuit boards possess properties fulfilling the demands of high-frequency microelectronics, providing substantial resistance to drop-impact induced damage.

Due to the high density of interfaces in these multilayers, interface-related effects become increasingly significant as the individual layer thickness decreases to the nanometer scale [8, 12, 18]. Extensive research has focused on interface-modulated strengthening, which is influenced by several factors, including Koehler stress [13], coherency stress [12, 21], lattice mismatch [22–24], stacking fault energy mismatch [3], and slip continuity [26]. Specifically, Koehler stress arises from the elastic modulus mismatch between adjacent layers [13], whereas coherency stress depends on lattice continuity across interfaces [12, 21].

Although many studies on interface-modulated strengthening employs multilayers composed of pure metal, the strengthening mechanisms in alloy-containing multilayers

Ruth Schwaiger was an editor of this journal during the review and decision stage. For the MRS Advances policy on review and publication of manuscripts authored by editors, please refer to http://mrs.org/editor-manuscripts.

✉ Xi Li
xi.li1@fz-juelich.de

Thomas Kreuter
thomas.kreuter@freseniusmedicalcare.com

Xuemei Luo
xmluo@hhu.edu.cn

Guangping Zhang
gpzhang@imr.ac.cn

Ruth Schwaiger
r.schwaiger@fz-juelich.de

[1] Institute of Energy Materials and Devices (IMD), Structure and Function of Materials (IMD-1), Forschungszentrum Jülich GmbH, 52425 Jülich, Germany

[2] Institute for Applied Materials (IAM), Karlsruhe Institute of Technology (KIT), Hermann-von-Helmholtz-Platz 1, 76344 Eggenstein-Leopoldshafen, Germany

[3] National Engineering Research Center for High Performance Homogenized Alloys, Institute of Metal Research, Chinese Academy of Sciences, 72 Wenhua Road, Shenyang 110016, People's Republic of China

often lack comprehensive quantitative description [29, 30]. Alloying elements, in particular, provide a crucial means to quantitatively investigate how diverse physical properties tune the strengthening effect.

Alloying is a well-established strengthening strategy in bulk materials, enhancing properties via multiple mechanisms including modulus mismatch tuning, solid solution strengthening, and precipitation hardening. These mechanisms can also affect lattice mismatch, which is prevalent in engineering materials with coherent or semi-coherent interfaces—such as matrix/precipitate systems, composition gradients across diffusion zones, and alternating layers in nanolaminates [4, 27, 28]. The lattice mismatch determines the structure and stress state of interface, which directly influences the microstructure and mechanical properties. Changing the lattice mismatch can vary the distribution of misfit dislocation and precipitation [6, 17] at interface, leaving a corresponding change of barrier to the movement of dislocations.

Among common multilayer systems, Cu/Ni is a model due to their similar lattice parameters and excellent interface quality. Ag is partly miscible with Cu and immiscible with Ni, ensuring it remains within the Cu layers [19, 20]. However, introducing Ag into Cu is known to expand the Cu lattice [2, 16], raising the question of whether such alloying could be used to modulate interface properties and enhance the strength of Cu/Ni multilayers.

Previous atomic-scale simulations predicted a ~ 20% and ~ 25% increase of the flow stress in biaxial tensile deformation for Cu–5%Ag/Ni and Cu–10%Ag/Ni, respectively, comparing with Cu/Ni multilayers. The increasing Ag content enhances strength via Ag precipitation and elevated misfit dislocation density at the Cu/Ni interface [10].

In this study, we synthesized Cu–xAg/Ni multilayers ($x = 0, 5, 10$ at.%) via magnetron sputtering at a substrate temperature of 100 °C, with an additional Cu–10 at.%Ag/Ni sample deposited at 300 °C. Nanoindentation was used to evaluate the mechanical properties, and microstructural characterization was performed to understand the relationship between Ag content, interface structure , and strengthening mechanisms. We hypothesize that Ag-induced lattice mismatch will enhance interface strengthening in a quantifiable and controllable manner.

Materials and Methods

Cu–xAg/Ni multilayers ($x = 0$ at.%, 5 at.%, 10 at.%) were deposited via DC magnetron sputtering onto 525 µm-thick single-crystal Si substrates at a deposition rate of 0.3 nm/s. The chamber was evacuated in an Ar atmosphere at a working pressure of 0.4 Pa, with a base pressure below 1×10^{-7} Torr. The materials of targets are Cu (purity ≥ 99.9999%), Ni (purity ≥ 99.995%), Cu–5 at.% Ag alloy (purity ≥ 99.99%) and Cu–10 at.% Ag alloy (purity ≥ 99.99%).

To optimize the deposition quality of the Cu–Ag layers, the substrate temperature was varied. Specifically, the Cu–10 at.% Ag/Ni multilayers were deposited at both 100 and 300 °C, while all other multilayers were deposited at 100 °C. Each multilayer consisted of individual layers 25 nm thick, with a total film thickness of 1000 nm.

Nanoindentation testing was carried out using a Nano Indenter G200 (Agilent/Keysight Technologies, Inc., California, USA) equipped with a diamond Berkovich tip and operated in continuous stiffness measurement (CSM) mode, with a constant strain rate of 0.05 s^{-1} at room temperature. The instrument was calibrated using a fused silica standard, and the tip area function and frame stiffness was verified prior to testing. Tests were performed when the thermal drif was below 0.05 nm/s. Fifteen indents were performed for each sample. To minimize substrate and surface effects, final hardness and modulus values were taken as the average within the indentation depth range of 90 nm–120 nm.

X-ray diffraction (XRD) analysis was conducted using a Rigaku D/max 2400 system with Cu/K-alpha radiation (λ = 1.54056 Å) in θ–2θ geometry with a scan range of 30–68°, step size of 0.02°, and a scan rate of 8°/min.

Transmission electron microscopy (TEM) samples were prepared by mechanical grinding followed by ion polishing at − 100 °C using a Gatan 691 precision ion polishing system. Cross-sectional microstructures were examined using a field emission TEM (FEI Tecnai F20), and elemental distributions were mapped using energy-dispersive X-ray spectroscopy (EDS) in scanning TEM (STEM) mode. STEM-EDS was performed at 200 kV with a dwell time of 1 µs/pixel and spatial resolution of 4.13 nm.

Results

The XRD patterns of Cu–xAg/Ni ($x = 0$ at.%, 5 at.%, 10 at.%) multilayers deposited at 100 °C, along with a Cu–10 at.% Ag/Ni multilayer deposited at 300 °C, are shown in Fig. 1a. All samples exhibit reflections corresponding to (111) and (200) planes of both Cu and Ni. For the sample deposited at 300 °C, an additional (111) Ag peak is observed, indicating Ag precipitation, whereas no Ag peak is detected in samples grown at 100 °C. The (111) peak position for Ni remains unchanged across all samples, while the (111) Cu peak shifts with increasing Ag content, suggesting expansion due to Ag incorporation.

The interplanar spacing of Cu d_{Cu} was calculated from the Cu(111) reflection, and the degree of lattice expansion, defined as d_{Cu-Ag}–d_{Cu}, is plotted as a function of Ag content in Fig. 1b. The lattice expansion values for films deposited at 100 °C deviate from Vegard's law [25] but align closely with

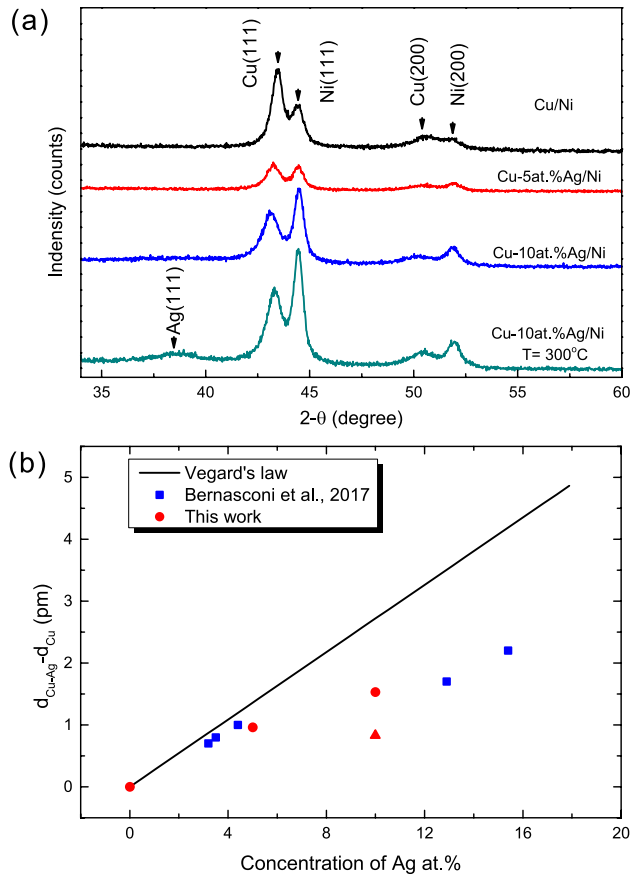

Fig. 1 X-ray diffraction (XRD) analysis and lattice expansion of Cu–xAg/Ni multilayers. **a** XRD patterns of Cu–xAg/Ni multilayers with $x = 0$ at.%, 5 at.%, 10 at.% deposited at 100 °C and Cu–10 at.% Ag/Ni deposited at 300 °C. Peaks corresponding to (111) and (200) planes of Cu and Ni are labeled; a distinct (111) Ag peak appears only in the 300 °C sample, indicating Ag precipitation. **b** Lattice expansion of the Cu layers as a function of Ag content, derived from the Cu (111) peak positions. Red circles correspond to samples deposited at 100 °C; the red triangle represents the 300 °C sample. Experimental data are compared with predictions from Vegard's law and with previous measurements on electrodeposited Cu–Ag alloys by Bernasconi et al. [2]

experimental results from Bernasconi et al. [2]. By contrast, the Cu–10 at.% Ag deposited at 300 °C shows significantly less lattice expansion, implying enhanced Ag demixing at higher deposition temperatures.

Cross-sectional TEM images of the Cu–5 at.% Ag/Ni and Cu–10 at.% Ag/Ni multilayers are shown in Fig. 2a, b. The layered structure is clearly visible, although contrast between the Cu–Ag and Ni layers is limited due to the similar atomic numbers. The bilayer period and columnar grain size were measured via TEM and are summarized in Table 1. The period thickness varies by less than 6.5%, and the grain size variation remains under 11%, indicating consistent deposition conditions across samples. A slight increase in average grain size is observed with increasing Ag content; however, this variation is not statistically significant relative to the standard deviation. Figure 2c, d show the STEM-HAADF images of Cu–5 at.% Ag/Ni and Cu–10 at.% Ag/Ni, with corresponding EDS elemental maps of Cu, Ag, and Ni. The Ag distribution contours in Fig. 2e, f confirm that Ag is primarily localized within the Cu–Ag layers. Horizontal integration of the EDS data reveals that while the average Ag concentration matches the target values, localized regions show significantly higher concentrations—up to twice the nominal content—indicating nanoscale Ag segregation.

High-resolution TEM (HRTEM) images (Fig. 3a, b) taken along the [110] zone axis reveal coherent interfaces between the Cu–Ag and Ni layers, oriented parallel to the (111) plane. Due to the similar atomic structure and Z-contrast of Cu–Ag and Ni, the interface location is estimated from bright-field (BF) TEM images. The FFT patterns in the insets confirm the orientation relationship $(111)_{Cu-Ag} \parallel (111)_{Ni}$. This relationship, which establishes a coherent interface parallel to the (111) plane, remains consistent across all samples.

Nanoindentation measurements were performed to evaluate the hardness and modulus of Cu–xAg/Ni multilayers. Figure 4a shows the hardness as a function of indentation depth (h_c). At shallow depths (below 50 nm), an elevated hardness is observed due to surface effects. In the 90–120 nm depth range, a plateau was reached, from which average modulus and hardness values were determined (Fig. 4b). The modulus values closely follow the rule-of-mixtures (ROM) prediction and decrease slightly with increasing Ag content. Conversely, hardness increases with Ag content, indicating strengthening. Compared to the pure Cu/Ni multilayer, the Cu–5 at% Ag/Ni and Cu–10 at% Ag/Ni multilayers show hardness increases of 10.4% and 12.9%, respectively.

Discussion

As shown in Fig. 1b, the measured lattice expansion of the Cu–Ag alloy in Cu–xAg/Ni multilayers is consistently lower than predicted by Vergard's law, particularly at higher Ag concentrations. This deviation suggests partial demixing of Ag atoms. Notably, the Cu–10 at.% Ag/Ni multilayer deposited at 300 °C shows significantly lower lattice expansion than its 100 °C counterpart, indicating that higher substrate temperatures promote further Ag demixing.

Using the measured lattice expansion and applying Vergard's law, the dissolved Ag content in the Cu matrix at 100 °C is estimated to be approximately 4.6 at.% and 7.3 at.% for the nominal 5 at.% and 10 at.% alloy, respectively. The remaining Ag is likely present as precipitates, which do not contribute to lattice expansion. While the absence of distinct Ag peaks in XRD limits direct analysis of these precipitates, the trends align with observations reported by

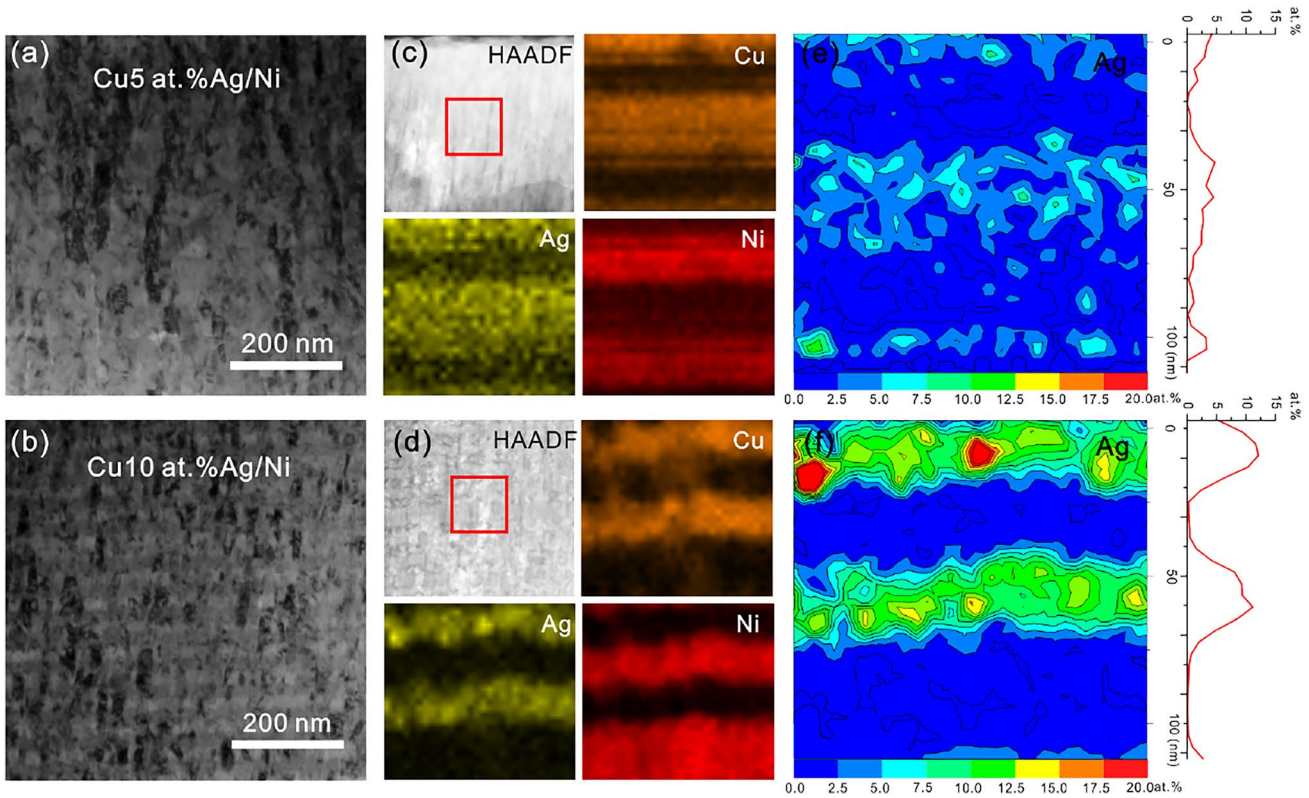

Fig. 2 Cross-sectional imaging and elemental mapping of Cu–xAg/Ni multilayers. **a, b** Bright-field (BF) TEM images of Cu–5 at.%Ag/Ni and Cu–10 at.%Ag/Ni, respectively. **c, d** Corresponding cross-sectional STEM-HAADF images, with red boxes indicating regions selected for EDS elemental mapping of Cu, Ag, and Ni. **e, f** Contour maps of Ag atomic concentration in the Cu–5 at.% Ag/Ni and Cu–10 at.% Ag/Ni multilayers, derived from the EDS maps shown in (**c**) and (**d**), respectively. The line profiles adjacent to each contour map represent horizontally integrated Ag concentration across the multilayer. Ag is primarily localized within the Cu–Ag layers, displaying Ag enrichment in nanoscale regions, particularly in the Cu–10 at% Ag/Ni sample.

Table 1 Bilayer period thickness and columnar grain size of each type of Cu–Ag/Ni multilayer measured by morphology in TEM. (Columnar grain size was determined by measuring over 200 individual grains per sample)

Sample	Substrate temperature (°C)	Period thickness (nm)	Columnar grain size (nm)
Cu/Ni	100	48.5 ± 6.7	25.9 ± 3.9
Cu–5 at.% Ag/Ni	100	51.8 ± 8.2	26.8 ± 6.1
Cu–10 at.% Ag/Ni	100	51.2 ± 6.9	29.0 ± 5.6
Cu–10 at.% Ag/Ni	300	51.7 ± 4.9	27.8 ± 8.6

Bernasconi et al. [2], suggesting a comparable precipitation behavior in electrodeposited Cu–Ag alloys.

Further confirmation is provided by EDS mapping in Fig. 2e, f, which reveals nanoscale Ag segregation within the Cu–Ag layers. Although the spatial resolution of EDS limits quantitative analysis, the presence of localized Ag-rich regions is clear. This segregation is consistent with the known limited solubility of Ag in Cu (< 0.1 wt.% at 200 °C [7]). Similar segregation behavior has also been predicted by atomistic simulations from Gola et al. [10], where Ag clustering was found both within the Cu layers and partially at the Cu/Ni interface.

Compared to the Cu/Ni multilayer, the Cu–Ag/Ni system benefits from additional strengthening contributions: solid solution strengthening (σ_{ss}), precipitation strengthening (σ_p), and an increase in interface barrier stress due to Ag-induced modifications ($\Delta\tau_i$). The total yield strength σ_y of the Cu–Ag/Ni multilayer can be expressed as:

$$\sigma_y = \sigma_{Cu/Ni} + \sigma_{ss} + \sigma_p + M\Delta\tau_i, \quad (1)$$

where $M = 3.06$ is the Taylor factor. Each term is discussed in detail below.

(1) $\sigma_{Cu/Ni}$: Yield strength of Cu/Ni, which is estimated from the hardness using $\sigma = H/3$.
(2) σ_{ss}: Calculated using Fleischer's model for dilute solid solutions [9], where:

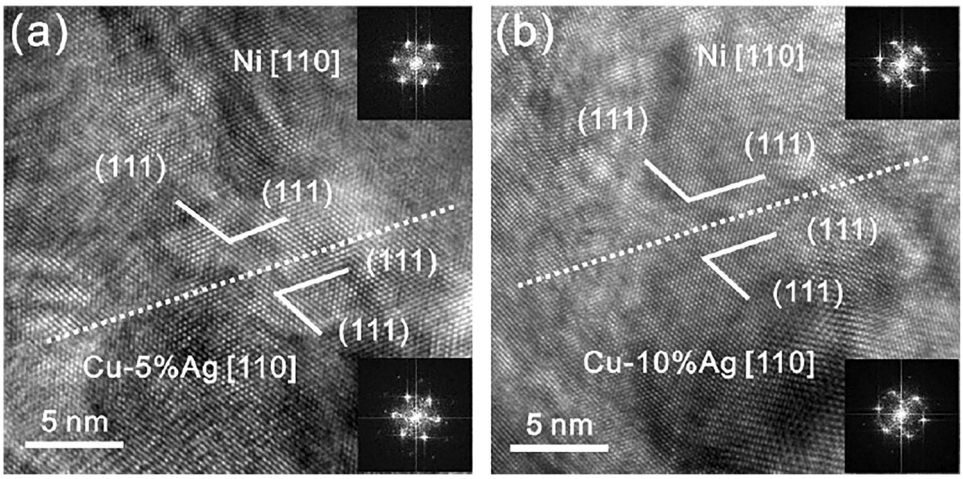

Fig. 3 High-resolution TEM (HRTEM) images of Cu–xAg/Ni multilayers taken along the [110] zone axis. **a** Cu–5 at.% Ag/Ni and **b** Cu–10 at.% Ag/Ni. The dashed lines mark the interfaces between the Cu–Ag and Ni layers, which appear coherent and are aligned parallel to the (111) crystallographic planes in both phases. The fast Fourier transform (FFT) patterns used to identify the crystal structure of Ni and Cu–xAg layers are displayed in the upper and lower insets, respectively. The observed orientation relationship is $(111)_{\mathrm{Cu-Ag}} \parallel (111)_{\mathrm{Ni}}$, indicating well-matched lattice planes across the interface

$$\sigma_{ss} = M\frac{G\epsilon^{\frac{3}{2}}\sqrt{c}}{700}, \tag{2}$$

with mismatch factor $\epsilon = |\frac{\epsilon_G}{1+0.5\epsilon_G} - \beta\epsilon_a|$, incorporating modulus (ϵ_G) and lattice (ϵ_a) mismatches. Here, G is the shear modulus of Cu, c is the concentration of solute Ag atoms, and $\beta = 3$.

(3) σ_p: Although Ag precipitation is confirmed, its contribution is difficult to quantify. Literature suggests solid solution strengthening dominates at low Ag content [2, 5], while precipitation hardening has a lesser impact, especially below 10–12 wt.% Ag.

(4) $\Delta\tau_i$: The additional interface barrier stress due to Ag alloying includes contributions from modulus mismatch (τ_G) [13] and lattice mismatch (τ_a) [23]:

$$\begin{aligned}\Delta\tau_i = \Delta\tau_G + \Delta\tau_a = \tau_G|_{\mathrm{Cu-Ag/Ni}} - \tau_G|_{\mathrm{Cu/Ni}} \\ + \tau_a|_{\mathrm{Cu-Ag/Ni}} - \tau_a|_{\mathrm{Cu/Ni}}.\end{aligned} \tag{3}$$

The expressions for τ_G and τ_a are:

$$\tau_G = \frac{G_1(G_2 - G_1)\sin\phi}{8\pi(G_1 + G_2)}, \tag{4}$$

$$\tau_a = \alpha G(\frac{\delta a}{a} - \frac{b}{2h}) \tag{5}$$

where $\alpha = 0.5$, G_1 and G_2 are the shear moduli of Cu–xAg and Ni, respectively, and h, b and ϕ are the layer thickness, Burgers vector, and slip/interface angle. Employing the XRD measured lattice parameter, lattice mismatch values were calculated as 2.56%, 3.03% and 3.31% for $x = 0, 5$, and 10 at.% Ag, respectively.

The calculated and experimental values for different strengthening contributions are summarized in Table 2. All mechanisms show increasing contributions with higher Ag content. While τ_G increases modestly, τ_a exhibits a more pronounced rise, emphasizing the role of lattice mismatch in strengthening.

Figure 4c visualizes the relative contributions. Solid solution strengthening and modulus mismatch contribute modestly, while precipitation strengthening appears minimal. Lattice misfit strengthening is the dominant mechanism. However, the calculated total strength slightly overestimates the experimental values. The discrepancy likely stems from simplifications in the theoretical model. The lattice misfit strengthening model by Rao et al. [23] assumes a 2D dislocation network at the interface, whereas atomic-scale simulations by Gola et al. [10] reveal a more complex 3D dislocation structure when Ag is present. These dislocation networks are further pinned by Ag atoms, increasing local stress barriers. Such 3D effects are not captured in simplified models, explaining the overestimation.

Conclusion

This study demonstrates that alloying Cu/Ni multilayers with Ag significantly enhances their mechanical performance through multiple synergistic strengthening mechanisms. The addition of Ag increases the lattice mismatch at the Cu/Ni interface—from 2.56% in pure Cu to 3.31% at 10 at.% Ag—while also promoting the formation of fine Ag-rich precipitates. These

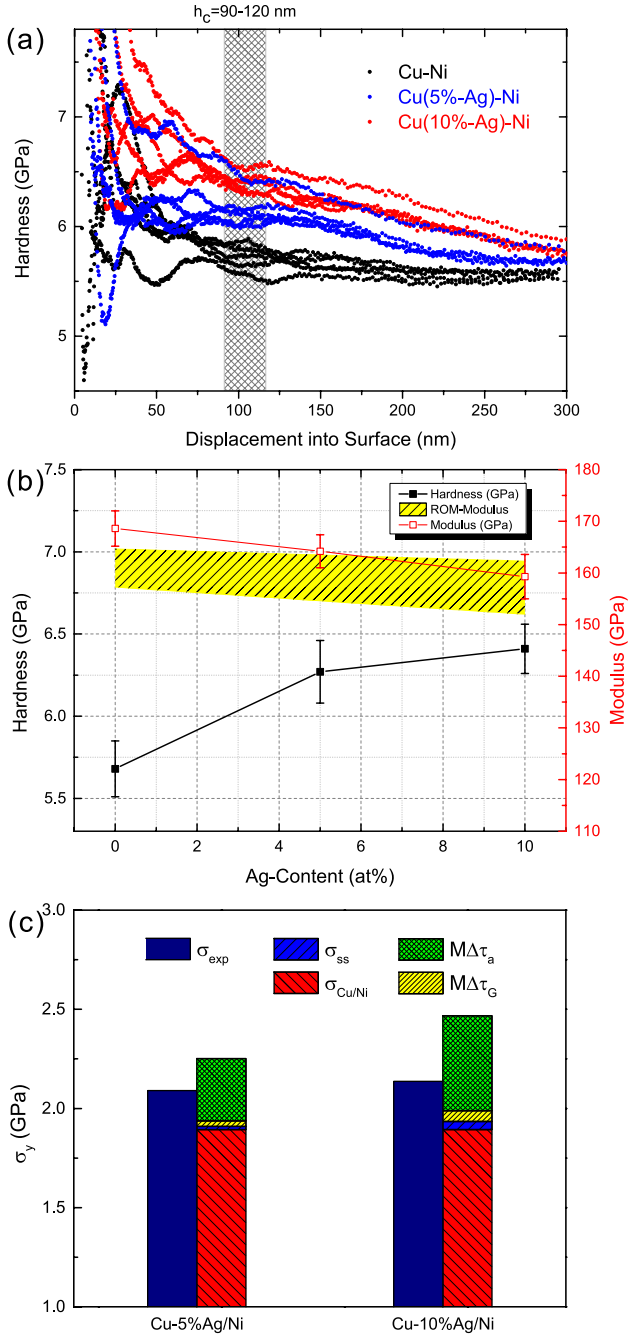

Fig. 4 Nanoindentation results for Cu–xAg/Ni multilayers ($x = 0$ at.%, 5 at.%, 10 at.%). **a** Hardness as a function of indentation depth (h_c). At shallow depths (< 50 nm), surface effects cause artificially high hardness values while a stable plateau is reached in the 90–120 nm range. **b** Average hardness and modulus values calculated within the 90–120 nm depth range. Error bars represent the standard deviation among 15 indentations per sample. The yellow shaded region indicates the range of elastic modulus values predicted by the rule-of-mixtures (ROM) for each composition. Increasing Ag content results in a clear increase in hardness, while the modulus shows a slight decreasing trend. **c** Comparison between experimental measurements and theoretical calculations of the strengthening contributions in Cu–xAg/Ni multilayers

Table 2 Experimental and calculated mechanical properties of Cu–xAg/Ni multilayers ($x = 0, 5,$ and10 at.%)

Sample	σ_{exp}	σ_{ss}	τ_G	τ_a
Cu/Ni	1893	0.0	407	441
Cu–5 at.% Ag/Ni	2090	33.6	416	542
Cu–10 at.% Ag/Ni	2136	82.5	425	594

All values are reported in MPa

structural changes lead to a measurable increase in hardness by up to 12.9%, as shown by nanoindentation testing. Our analysis reveals that while solid solution and precipitation strengthening contribute, the dominant mechanism is interface strengthening driven by lattice misfit. This finding is supported by theoretical modeling, though the models slightly overestimate strength due to simplifications in representing the dislocation network.

These results underscore the importance of alloy design in tuning interface properties and mechanical performance in nanoscale multilayer systems. Specifically, they highlight lattice mismatch as a powerful and controllable parameter for enhancing strength at the nanoscale. This insight provides a framework for the rational design of high-performance nanolayered composites in structural and functional applications where mechanical reliability at reduced dimensions is critical.

Acknowledgments Dr. Xi Li gratefully acknowledges the support from the Alexander von Humboldt Foundation through a Humboldt Research Fellowship.

Author contributions XLi: Writing—original draft, data curation, formal analysis, investigation, methodology, validation, and visualization. TK: Data curation, investigation, formal analysis, validation, and visualization. XLuo: Data curation, review and editing (supporting), formal analysis, and investigation. GZ: Writing—review and editing, conceptualization, funding acquisition, methodology, project administration, resources, and supervision. RS: Writing—review and editing; conceptualization, funding acquisition, methodology, project administration, resources, and supervision.

Funding Open Access funding enabled and organized by Projekt DEAL. This work was supported by the National Natural Science Foundation of China (NSFC, Grant Nos. 51571199, 51601198 and 51771207).

Data availability The datasets used during the current study are available from the corresponding author on reasonable request.

Declarations

Conflict of interest On behalf of all authors, the corresponding author states that there is no conflict of interest.

References

1. D. Aurongzeb, M. Holtz, J.M. Berg et al., The influence of interface roughness on electrical transport in nanoscale metallic multilayers. J. Appl. Phys. **98**(6), 063708 (2005). https://doi.org/10.1063/1.2058172
2. R. Bernasconi, J.L. Hart, A.C. Lang et al., Structural properties of electrodeposited Cu–Ag alloys. Electrochim. Acta **251**, 475–481 (2017). https://doi.org/10.1016/j.electacta.2017.08.097
3. D. Bufford, Z. Bi, Q. Jia et al., Nanotwins and stacking faults in high-strength epitaxial Ag/Al multilayer films. Appl. Phys. Lett. **101**(22), (2012). https://doi.org/10.1063/1.4768000
4. M. Chisholm, D. Shin, G. Duscher et al., Atomic structures of interfacial solute gateways to θ' precipitates in Al–Cu alloys. Acta Mater. **212**, 116891 (2021). https://doi.org/10.1016/j.actamat.2021.116891
5. H. Cho, B.S. Lee, H.H. Jo, Development of high strength and high conductivity Cu–Ag alloy for medical ultrasound equipment. Surf. Rev. Lett. **17**(01), 93–97 (2010). https://doi.org/10.1142/S0218625X10013953
6. W. Chrominski, M. Lewandowska, Influence of dislocation structures on precipitation phenomena in rolled Al–Mg–Si alloy. Mater. Sci. Eng. A **793**, 139903 (2020). https://doi.org/10.1016/j.msea.2020.139903
7. R.P. Elliott, F.A. Shunk, W.C. Giessen, The Ag–Cu (silver-copper) system. Bull. Alloy Phase Diagrams **1**(1), 41–45 (1980). https://doi.org/10.1007/BF02883284
8. L. Fang, L.H. Friedman, Analytic treatment of metallic multilayer strength at all length scales: Influence of dislocation sources. Acta Mater. **55**(5), 1505–1514 (2007). https://doi.org/10.1016/j.actamat.2006.10.012
9. R.L. Fleischer, Substitutional solution hardening. Acta Metall. **11**(3), 203–209 (1963). https://doi.org/10.1016/0001-6160(63)90213-X
10. A. Gola, P. Gumbsch, L. Pastewka, Atomic-scale simulation of structure and mechanical properties of abcd $Cu_{1-x}Ag_x$|ni multilayer systems. Acta Mater. **150**, 236–247 (2018). https://doi.org/10.1016/j.actamat.2018.02.046
11. W. Han, M.J. Demkowicz, N.A. Mara et al., Design of radiation tolerant materials via interface engineering. Adv. Mater. **25**(48), 6975–6979 (2013). https://doi.org/10.1002/adma.201303400
12. R. Hoagland, T. Mitchell, J. Hirth et al., On the strengthening effects of interfaces in multilayer fee metallic composites. Philos. Mag. A **82**(4), 643–664 (2002). https://doi.org/10.1080/01418610208243194
13. J. Koehler, Attempt to design a strong solid. Phys. Rev. B **2**(2), 547 (1970). https://doi.org/10.1103/PhysRevB.2.547
14. N. Lebbad, J. Voiron, B. Nguyen et al., Electrodeposition of metallic multilayers with modulated electric regimes. Thin Solid Films **275**(1), 216–219 (1996). (papers presented at the European Materials Research Society 1995 Spring Conference, Symposium E: Structure and Properties of Metallic Thin Films and Multilayers). https://doi.org/10.1016/0040-6090(95)07047-8
15. N. Li, M. Martin, O. Anderoglu et al., He ion irradiation damage in Al/Nb multilayers. J. Appl. Phys. **105**(12), 123522 (2009). https://doi.org/10.1063/1.3138804
16. S. Mader, Metastable alloy films. J. Vacuum Sci. Technol. **2**(1), 35–41 (1965). https://doi.org/10.1116/1.1492396
17. H. Mao, C. Zeng, Z. Zhang et al., The effect of lattice misfits on the precipitation at dislocations: phase-field crystal simulation. Materials **16**(18), 6307 (2023). https://doi.org/10.3390/ma16186307
18. A. Misra, J. Hirth, R. Hoagland, Length-scale-dependent deformation mechanisms in incoherent metallic multilayered composites. Acta Mater. **53**(18), 4817–4824 (2005). https://doi.org/10.1016/j.actamat.2005.06.025
19. B. Predel, Ag–Cu (silver-copper), in *Landolt-Börnstein—Group IV Physical Chemistry*, ed. by O. Madelung, vol 5a (Springer, Berlin, 1991b). https://doi.org/10.1007/10000866_23
20. B. Predel, Cu–Ni (copper-nickel), in *Landolt-Börnstein—Group IV Physical Chemistry*, ed. by O. Madelung, vol 5d (Springer, Berlin, 1991b). https://doi.org/10.1007/10086090_1095
21. V. Ramaswamy, W. Nix, B. Clemens, Coherency and surface stress effects in metal multilayers. Scripta Mater. **50**(6), 711–715 (2004). https://doi.org/10.1016/j.scriptamat.2003.11.037
22. S. Rao, P. Hazzledine, Atomistic simulations of dislocation–interface interactions in the Cu–Ni multilayer system. Philos. Mag. A **80**(9), 2011–2040 (2000). https://doi.org/10.1080/01418610008212148
23. S. Rao, P. Hazzledine, D. Dimiduk, Interfacial strengthening in semi-coherent metallic multilayers. MRS Online Proc. Library (OPL) **362**, 67 (1994). https://doi.org/10.1557/PROC-362-67
24. S. Shao, J. Wang, A. Misra et al., Spiral patterns of dislocations at nodes in (111) semi-coherent fcc interfaces. Sci. Rep. **3**(1), 2448 (2013). https://doi.org/10.1038/srep02448
25. L. Vegard, Die konstitution der mischkristalle und die raumfüllung der atome. Z. Phys. **5**(1), 17–26 (1921). https://doi.org/10.1007/BF01349680
26. J. Wang, A. Misra, R. Hoagland et al., Slip transmission across fcc/bcc interfaces with varying interface shear strengths. Acta Mater. **60**(4), 1503–1513 (2012). https://doi.org/10.1016/j.actamat.2011.11.047
27. S. Wang, T. Wen, J. Han et al., Coherent and semicoherent α/β interfaces in titanium: structure, thermodynamics, migration. npj Comput. Mater. **9**(1), 216 (2023). https://doi.org/10.1038/s41524-023-01170-w
28. W. Wu, M. Gong, B. Wei et al., Atomistic modeling of interface strengthening in Al–Si eutectic alloys. Acta Mater. **225**, 117586 (2022). https://doi.org/10.1016/j.actamat.2021.117586
29. X. Zhang, A. Misra, H. Wang et al., Enhanced hardening in Cu/330 stainless steel multilayers by nanoscale twinning. Acta Mater. **52**(4), 995–1002 (2004). https://doi.org/10.1016/j.actamat.2003.10.033
30. Y. Zhao, J. Zhang, Y. Wang et al., Unusual plastic deformation behavior of nanotwinned Cu/high entropy alloy FeCoCrNi nanolaminates. Nanoscale **11**(23), 11340–11350 (2019). https://doi.org/10.1039/C9NR00836E